Precision Engineering 38 (2014) 799–808

Contents lists available at ScienceDirect

Precision Engineering

journal homepage: www.elsevier.com/locate/precision

Value of information-based experimental design: Application to process damping in milling

Jaydeep M. Karandikar[a], Christopher T. Tyler[a], Ali Abbas[b], Tony L. Schmitz[a,*]

[a] Mechanical Engineering and Engineering Science, University of North Carolina at Charlotte, Charlotte, NC, United States
[b] Industrial and Systems Enterprise Engineering, University of Illinois at Urbana-Champaign, Urbana, IL, United States

ARTICLE INFO

Article history:
Received 8 July 2013
Received in revised form 7 January 2014
Accepted 18 April 2014
Available online 24 April 2014

Keywords:
Milling
Process damping
Bayesian inference
Value of information
Experimental design

ABSTRACT

This paper describes a value of information-based experimental design method that uses Bayesian inference for belief updating. The application is process damping coefficient identification in milling. An analytical process damping algorithm is used to model the prior distribution of the stability boundary (between stable and unstable cutting conditions). The prior distribution is updated using experimental results via Bayesian inference. The updated distribution of the stability boundary is used to determine the posterior process damping coefficient value. A value of information approach for experimental test point selection is then demonstrated which minimizes the number of experiments required to determine the process damping coefficient. Subsequent experimental parameters are selected such that the percent reduction in the standard deviation of the process damping coefficient is maximized. The method is validated by comparing the process damping posterior values to residual sum of squares results using a grid-based experimental design approach. Results show a significant reduction in the number of experiments required for process damping coefficient parameter determination. The advantages of using the value of information approach over the traditional design of experimental methods are discussed.

1. Introduction

Traditional design of experiment (DOE) approaches, such as factorial design, response surface methodology, and Taguchi orthogonal arrays, find widespread applications in engineering testing. DOE is used to reduce input parameter uncertainty, evaluate the effects and interactions of input parameters on the output, and test hypotheses [1,2]. The goal is to optimize the number of experiments required to achieve a desired output. In this paper, a value of information method for experimental selection using Bayesian inference is described to reduce input parameter uncertainty. The selected application is experimental identification of the process damping coefficient in milling. Value of information is defined as the expected profit before testing minus the profit after testing or, in terms of cost, the cost prior to testing minus the expected cost after testing.

The fundamental principle governing the value of information method is that an experiment is only worthwhile if the value gained from the experiment is more than the cost of performing the experiment [3]. Therefore, the experimental test point is selected which adds the most (expected) value. Note that, while the value of information uses expected value after testing, it is calculated before actually performing the test. The approach considers the importance of uncertainty reduction to the decision maker by assigning a value to the information gained from an experiment [4]. Experimental design using value of information takes into account the probabilistic nature of the uncertainties along with their effect on the output [5].

In this study, the value of information method is used to design experiments for model parameter uncertainty reduction. Therefore, the value of information is modified as parameter uncertainty, expressed in terms of the standard deviation, before testing minus the expected uncertainty after testing. Note that the value after testing calculation depends on the current state of information. Therefore, the value of information cannot be determined by any method which does not explicitly take into account the state of information [3]. To this effect, Bayesian inference is a formal and normative method of combining experimental evidence with the current state of information to determine updated beliefs regarding an uncertain variable. Coupling Bayesian inference with models enables a value to be placed on the information gained from an experiment prior to performing it.

The value of information method for experimental design has two distinct advantages over the traditional (statistical) DOE. First,

* Corresponding author. Tel.: +1 7046875086.
E-mail address: tony.schmitz@uncc.edu (T.L. Schmitz).

http://dx.doi.org/10.1016/j.precisioneng.2014.04.008
0141-6359/

statistical DOE does not consider the value of uncertainty reduction in experimental point selection. As noted, the experimental design can be optimized based on maximum value added to the current state of information. Second, the value of information can be used as a stopping criterion for performing additional experiments. If the expected cost of performing an experiment is more than the expected value to be gained from the experiment, it is not recommended that the experiment be completed. For example, the user can decide that an experiment is worthwhile only if there is at least a 10% reduction in the standard deviation of the input parameter, which is the cost of performing the experiment. This implies that if the value of information for an experiment is less than 10%, it is not worthwhile to perform the experiment. Traditional DOE typically requires a fixed number of experiments which are decided prior to any testing.

The remainder of the paper is organized as follows. Section 2 describes the process damping phenomenon in milling. Section 3 summarizes a grid-based experimental design approach to identify the process damping coefficient using a residual sum of squares (*RSS*) method. The experimental setup and results are provided. Section 4 describes the contrasting Bayesian inference procedure for updating process damping coefficient distributions. Section 5 describes the value of information method for experimental design. Section 6 provides conclusions.

2. Process damping in machining stability analysis

The analytical stability lobe diagram offers an effective predictive capability for selecting stable chip width-spindle speed combinations in machining operations [6–9]. However, the increase in allowable chip width provided at spindle speeds near integer fractions of the system's dominant natural frequency is diminished substantially at low spindle speeds where the stability lobes are closely spaced. For these low speeds, the process damping effect can serve to increase the chatter-free chip widths. This increased stability at low spindle speeds is particularly important for hard-to-machine materials that cannot take advantage of the higher speed stability zones due to prohibitive tool wear at high cutting speeds. Many researchers have investigated process damping in turning and milling operations. Seminal studies were carried out by Wallace and Andrew [10], Sisson and Kegg [11], Peters et al. [12], and Tlusty [13]. It was suggested by this early work that interference contact between the flank of the cutting tool and wavy cutting surface contributes to the process damping phenomenon. The increased use of hard-to-machine alloys has driven recent efforts to accurately predict process damping behavior. Wu [14] developed a model in which plowing forces present during the tool–workpiece contact are assumed to be proportional to the volume of interference between the cutter flank face and undulations on the workpiece surface in turning. Elbestawi and Ismail [15], Lee et al. [16], Huang and Wang [17], and Ahmadi and Ismail [18] extended Wu's force model to milling operations. Budak and Tunc [19] and Altintas et al. [20] experimentally identified different dynamic cutting force models to include process nonlinearities and incorporate process damping. Tyler and Schmitz [21] described an analytical approach to establish the stability boundary that includes process damping effects in turning and milling operations using a single process damping coefficient. These studies described process damping as energy dissipation due to interference between the cutting tool clearance face and machined surface during relative vibrations between the tool and workpiece. It was shown that, given fixed system dynamics, the influence of process damping increases at low spindle speeds because the number of undulations on the machined surface between revolutions/teeth increases, which also increases the local slope of the wavy surface.

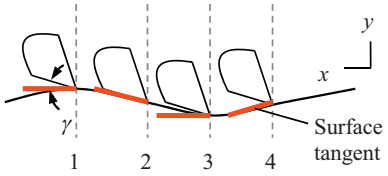

Fig. 1. Physical description of process damping. The clearance angle varies with the instantaneous surface tangent as the tool removes material on the sinusoidal surface.

This, in turn, leads to increased interference and additional energy dissipation.

2.1. Process damping description

To describe the physical mechanism for process damping, consider a tool moving on a sine wave while shearing away the chip [22]; see Fig. 1. Four locations are identified: (1) the clearance angle, γ, between the flank face of the tool and the work surface tangent is equal to the nominal relief angle for the tool; (2) γ is significantly decreased and can become negative (which leads to interference between the tool's relief face and surface); (3) γ is again equal to the nominal relief angle; and (4) γ is significantly larger than the nominal value.

At points 1 and 3 in Fig. 1, the clearance angle is equal to the nominal value so there is no effect due to cutting on the sinusoidal path. However, at point 2 the clearance angle is small (or negative) and the thrust force in the surface normal direction is increased. At point 4, on the other hand, the clearance angle is larger than the nominal and the thrust force is decreased. Because the change in force caused by the sinusoidal path is 90° out of phase with the displacement and has the opposite sign from velocity, it is considered to be a viscous damping force (i.e., a force that is proportional to velocity). Given the preceding description, the process damping force, F_d, in the y direction can be expressed as a function of velocity, $\dot{y}$, chip width, b, cutting speed, V, and a process damping constant C [21]. See Eq. (1).

$$F_d = -C\frac{b}{V}\dot{y} \tag{1}$$

Because the new damping value is a function of both the spindle speed-dependent limiting chip width and the cutting speed, the b and Ω vectors must be known in order to implement the new damping value. This leads to a converging stability analysis that incorporates process damping. The following steps are completed for each lobe in the stability lobe diagram:

1. the analytical stability boundary is calculated with no process damping ($C = 0$) to identify initial b and Ω vectors;
2. these vectors are used to determine the corresponding new damping coefficient vector (which includes both the structural damping and process damping, $C \neq 0$);
3. the stability analysis is repeated with the new damping coefficient vector to determine the updated b and Ω vectors;
4. the process is repeated until the stability boundary converges.

The automated algorithm description and validation are described in [21]. Fig. 2 illustrates a comparison between stability lobes diagrams developed with and without process damping for a selected C value.

3. Grid-based experimental design and results

As a first step in this study, the objective was to determine the process damping coefficient for milling with a particular

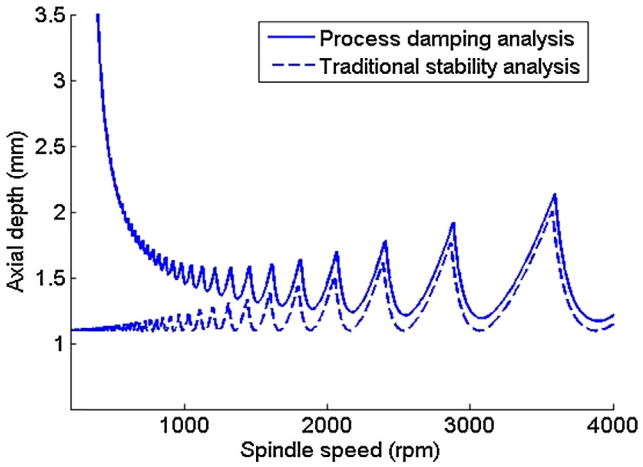

Fig. 2. Comparison between stability lobes with and without process damping.

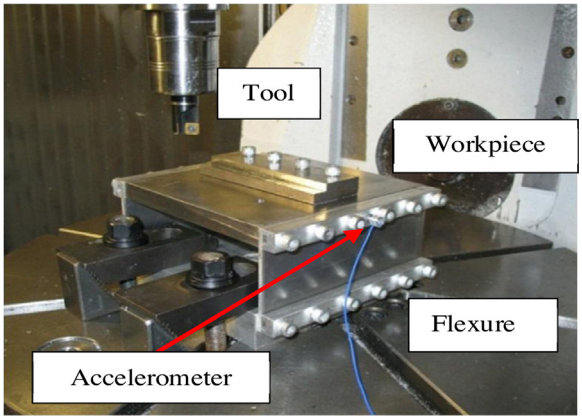

Fig. 3. Setup for milling stability tests. An accelerometer was used to measure the vibration signal during cutting.

tool–workpiece pair. Note that the experimental results were binary in nature; an experiment at an axial depth-spindle speed combination were either stable or unstable. Based on the stable/unstable cutting test results, a single variable residual sum of squares (*RSS*) estimation was applied to identify the process damping coefficient that best represented the experimental limiting axial depth of cut, b_{lim}. The spindle-speed dependent experimental stability limit, b_i, was selected to be the midpoint between the stable and unstable points at the selected spindle speed. The sum of squares of residuals is given by Eq. (2), where $f(\Omega_i)$ is the analytical stability boundary and j is the number of test points. A range of process damping coefficients was selected and the *RSS* value was calculated for each corresponding stability limit. The C value that corresponded to the minimum *RSS* value was selected to identify the final stability boundary for all test conditions [21].

$$RSS = \sum_{i=1}^{j} (b_i - f(\Omega_i))^2 \tag{2}$$

A first step in traditional DOE is to select the factors and number of levels. The factors influencing stability are axial depth and spindle speed for a given radial depth of cut. The process damping zone is identified here as the region where spindle speed is less than 1200 rpm. The spindle speed range extended from 200 rpm to 1100 rpm and was divided into 10 levels. The axial depth range for experiments was divided in five levels from 1 mm to 3 mm. Therefore, a grid of test points at low spindle speeds was selected to investigate the process damping behavior. The experimental design used here was full factorial; an experiment was performed at every grid point (for a total of 50 experiments). Note that alternative methods, such as randomized or Latin hypercube experimental design, will not work in this case because the *RSS* method requires both a stable and unstable result at each spindle speed. The number of experiments can be reduced by decreasing the number of levels in the spindle speed and axial depth range. However, since the process damping behavior in the range selected is not known, the preselected levels were deemed appropriate.

3.1. Experimental setup and results

In order to provide convenient control of the system dynamics, a single degree-of-freedom, parallelogram leaf-type flexure was constructed to provide a flexible foundation for individual AISI 1018 steel workpieces; see Fig. 3. Because the flexure compliance was much higher than the tool-holder–spindle-machine, the stability analysis was completed using only the flexure's dynamic properties. A radial immersion of 50% and a feed per tooth of 0.05 mm/tooth was used for all conventional (up) milling tests.

An accelerometer (PCB Piezotronics model 352B10) was used to measure the flexure's vibration during cutting. The frequency content of the accelerometer signal was used in combination with the machined surface finish to establish stable/unstable performance, i.e., cuts that exhibited significant frequency content at the flexure's compliant direction natural frequency, rather than the tooth passing frequency and its harmonics, were considered to be unstable.

As noted, stability tests were performed at all 50 grid points. The results of the coefficient identification method are depicted in Fig. 4 for an 18.54 mm diameter, single-tooth inserted endmill with a 15° relief angle. For the same milling conditions and system dynamics, the process was repeated for a 19.05 mm diameter, single-tooth inserted endmill with an 11 relief angle. The stability boundary for this experiment is provided in Fig. 5. The corresponding process damping coefficients and cutting force coefficients in the tangential, t, and normal, n, directions (as defined in Ref. [22]) are provided in Table 1.

The cutting force coefficients were identified using a linear regression on the mean forces in the x (feed) and y directions at different feed per tooth values. The cutting force was measured under stable cutting conditions using a cutting force dynamometer (Kistler model 9257B). For these tests, the insert wear was

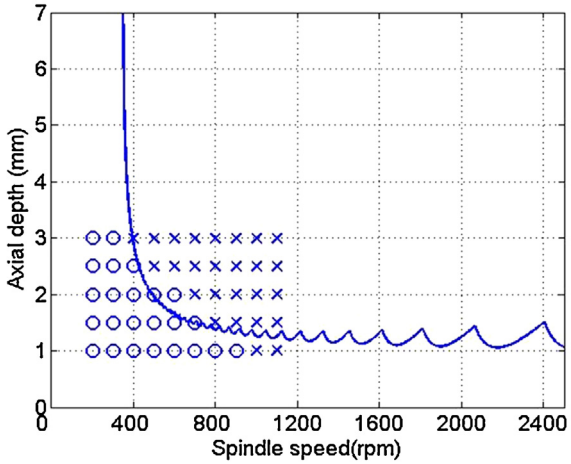

Fig. 4. Up milling stability boundary for 50% radial immersion, 18.54 mm diameter, 15° relief angle, low wear milling tests using the 228 Hz flexure setup ($C = 2.5 \times 10^5$ N/m).

Table 1
Comparison of process damping and cutting force coefficients for different relief angle cutters.

Relief angle (°)	C (N/m)	K_t (N/mm^2)	K_n (N/mm^2)
15	2.5×10^5	2111.2	1052.6
11	3.3×10^5	2234.9	1188.2

monitored using in-process optical flank wear measurements and the insert was replaced if the wear exceeded a predetermined value. From Figs. 4 and 5 it can be observed that numerous cutting tests were used to identify the process damping coefficient for a particular cutting operation. This can be costly if there are multiple cutter geometries or workpiece materials for which stability boundaries need to be constructed. The following section details a Bayesian updating method for optimizing the experimental test selection and determining the process damping coefficient more efficiently.

The selection of the maximum and minimum levels, the range of variables, and the number of levels are typically decided using rules of thumb and guesswork by the experimenter; these selections can represent limitations to traditional DOE methods. To illustrate, the total number of experiments may be reduced by selecting only three levels each for spindle speed and axial depth. However, if the result is stable (or unstable) for every test, there is no reduction in uncertainty in the process damping coefficient and the process has to be repeated using a different range and number of levels. Furthermore, in DOE the test parameters are decided prior to any testing and, therefore, do not take into account the value of reduction in uncertainty and the cost of performing the experiment. A value of information-based experimental design using Bayesian inference addresses these limitations.

4. Bayesian updating of the process damping coefficient

This section describes the Bayesian updating method for process damping coefficient identification. The updating was performed using the experimental results shown in Figs. 4 and 5. In these figures, uncertainty exists in the true location of the stability boundary due to the uncertainties/assumptions in the process damping model and its parameters as well as factors that are not known. Therefore, the stability boundary may be modeled as a cumulative probability distribution rather than a deterministic boundary. From a Bayesian standpoint, an uncertain variable is treated as random and is characterized by a probability distribution. Bayesian inference is a normative and formal method of belief updating when new information (e.g., experimental stability results) is made available. The stability boundary prediction proceeds by generating n sample paths, each of which may represent the actual stability boundary with some probability. For the prior (or initial belief), each path is assumed to be equally likely to be the true stability limit. Therefore, the probability that each sample path is the true stability limit is $1/n$. These sample paths are used as the prior in applying Bayesian inference. Bayesian updating was used to update the prior probability of sample paths given experimental result, and therefore, the process damping coefficient distribution. The entire methodology is defined as Bayesian updating using a random walk approach. Bayes' rule is given by the following equation.

$$P(path = true\ stability\ \lim it | test\ result) \propto P(test\ result | path = true\ stability\ \lim it)\, P(path = true\ stability\ \lim it) \quad (3)$$

Here $P(path = true\ stability\ limit)$ is the prior probability that a selected path is the true stability limit; before any testing; it is equal to $1/n$ for any sample path. Also, $P(test\ result \mid path = true\ stability\ limit)$ is the likelihood of obtaining the test result given the true stability limit. Their products yields the posterior probability that a selected path is the true path given the test result, $P(path = true\ stability\ limit \mid test\ result)$. In practice, the probability of the test result, $P(test\ result)$, may be used to normalize the posterior probability (by dividing the right hand side of Eq. (3) by this value). The sample paths are generated by randomly sampling from the prior distributions of the K_t, K_n, and C values and calculating a stability boundary for each set.

4.1. Establishing the prior

The random sample stability limits were generated by sampling from the prior distributions of K_t, K_n, and C. To demonstrate the approach, the 18.54 mm diameter, 11° relief angle tool is considered. The distribution of C is not known and has to be determined. The prior marginal distribution of C was selected to be the uniform distribution $U(0.5 \times 10^5,\ 10 \times 10^5)$, where the values in the parenthesis specify the lower and upper limits on C, respectively. A uniform distribution denotes that it is equally likely for the value of C to take any value between 0.5×10^5 N/m and 10×10^5 N/m and represents a non-informative case where little prior knowledge of the variable is available. In general, the prior marginal distribution of C is chosen based on all available information, such as literature reviews, prior experimental data, and/or expert opinions. In this study, because no specific information was available, a uniform prior was selected. Recall that the value of C for the 18.54 mm diameter, 15° relief angle tool was found to be 2.5×10^5 N/m using the *RSS* method (see Fig. 4). The values of K_t and K_n were calculated using a linear least squares fit to the mean forces in the x (feed) and y directions at different feed per tooth values. The mean and standard deviation of the force coefficients were calculated from three measurement sets. Based on this data, the marginal prior distributions of the force coefficients were $K_t = N(2111.2, 78.3)$ N/mm^2 and $K_n = N(1052.6, 27.9)$ N/mm^2, where N denotes a normal distribution and the terms in parenthesis specify the mean and standard deviation, respectively. The prior distributions of K_t, K_n, and C were assumed to be independent of each other. Although, K_t and K_n are most likely correlated, an independent assumption is chosen because it is conservative. Random samples (1×10^4) are drawn from the prior distributions and the stability limit was calculated for each sample. The probability that each sample stability limit is the true stability limit is 1×10^{-4}. Recall that for the prior, each stability limit was assumed to be equally likely to be the true limit. Fig. 6 shows the prior cumulative distribution function (cdf) for probability of stability. The maximum possible axial depth of cut possible was defined as 7.5 mm based on the tool's cutting edge

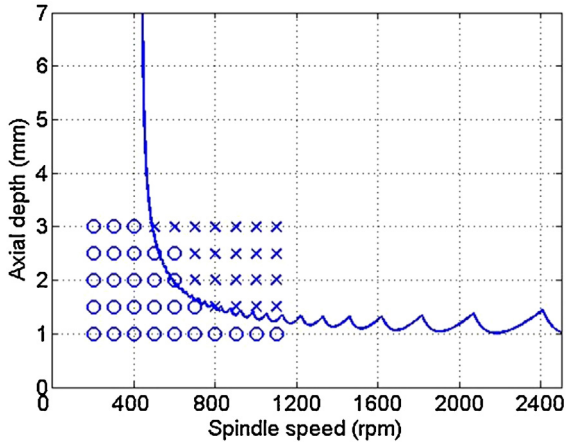

Fig. 5. Up milling stability boundary for 50% radial immersion, 19.05 mm diameter, 11° relief angle, low wear milling tests using the 228 Hz flexure setup ($C = 3.3 \times 10^5$ N/m).

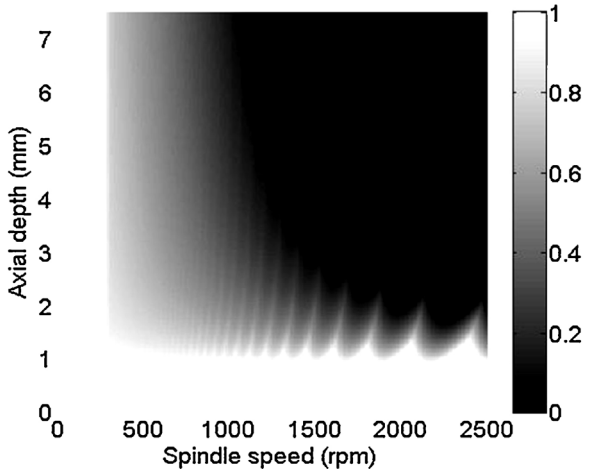

Fig. 6. Prior cdf of stability. The gray color scale represents the probability of stability for any spindle speed, axial depth combination (1/white is likely to be stable, while 0/black is unlikely to be stable).

length. Figs. 7 and 8 show the probability of stability, p(stability), as a function of axial depth at 400 rpm and 1000 rpm, respectively. As expected, the probability of stability decreases at higher axial depths at a given spindle speed. For example, the probability of stability at 1 mm is 1 at both speeds, while the probability of stability for an axial depth of 4 mm is 0.7 at 400 rpm and only 0.25 at 1000 rpm.

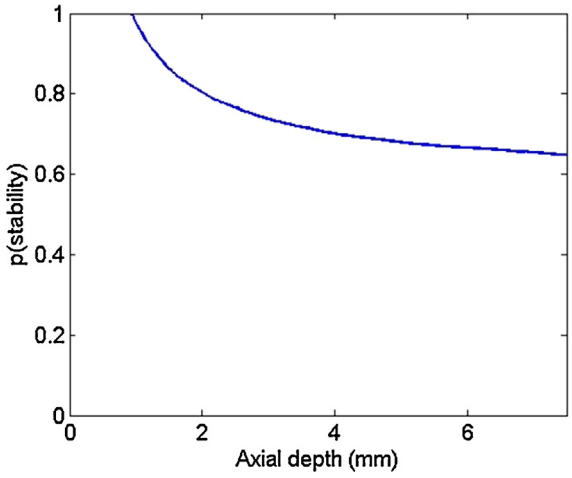

Fig. 7. Probability of stability at 400 rpm.

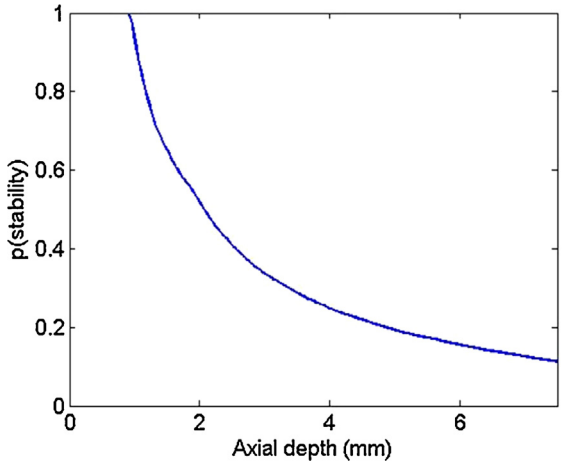

Fig. 8. Probability of stability at 1000 rpm.

4.2. Likelihood function

The likelihood function describes how likely the test result is given that the sample path is the true stability limit. The likelihood function incorporates the uncertainty in the process damping model and, therefore, the stability boundary. To illustrate, consider an experiment completed at a spindle speed of 1000 rpm and an axial depth of 3 mm. A stable result indicates that the test result is equally likely for all paths that have an axial depth greater than 3 mm at 1000 rpm; they are assigned a likelihood of unity. On the other hand, a stable result at 3 mm is unlikely for all paths with an axial depth less than 3 mm at 1000 rpm. Note that the stable result is unlikely, but not impossible for such paths, giving a nonzero likelihood. As shown in Figs. 4 and 5, stable points may lie above the boundary and unstable points may lie below the boundary since there is uncertainty in the stability boundary location. Note that the test result is increasingly unlikely for values less than 3 mm at 1000 rpm. For example, the test result is more unlikely for a path that has a value of 1 mm at 1000 rpm relative to a path that has a value of 2.5 mm at 1000 rpm. Therefore, the likelihood is a one-sided function. The likelihood function for a stable result is described by the following equation.

$$\begin{aligned} l &= e^{-(b-b_{test})^2/k} \quad b < b_{test} \\ &= 1 \qquad\qquad\quad b \geq b_{test} \end{aligned} \tag{4}$$

The likelihood function is expressed as a non-normalized normal distribution, where the parameter $k = 2\sigma^2$ and σ is the standard deviation in the axial depth due to the model uncertainty. The value of σ was taken to be 0.5 mm. Similarly, an unstable cut indicates that test result is likely for all paths that have an axial depth value less than 3 mm at 1000 rpm, while it is unlikely for all paths that have a value greater than 3 mm. Although a Gaussian kernel is used in this study, it can be any function defined by the user based on his/her beliefs. The likelihood function for an unstable result is provided in Eq. (5). Fig. 9 displays the likelihood function for a stable result at 3 mm and Fig. 10 shows the likelihood for an unstable result.

$$\begin{aligned} l &= 1 \qquad\qquad\quad b < b_{test} \\ &= e^{-(b-b_{test})^2/k} \quad b \geq b_{test} \end{aligned} \tag{5}$$

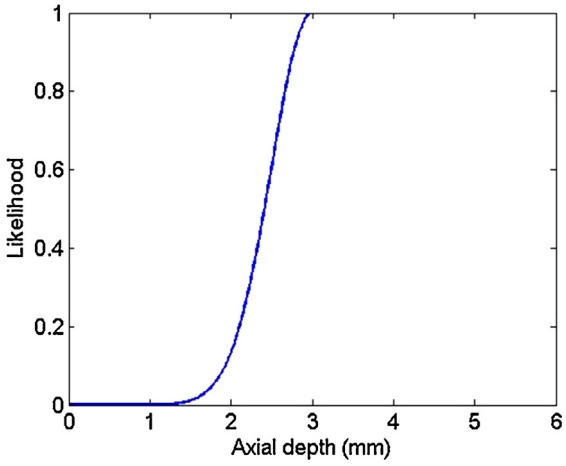

Fig. 9. Likelihood given a stable result at 3 mm.

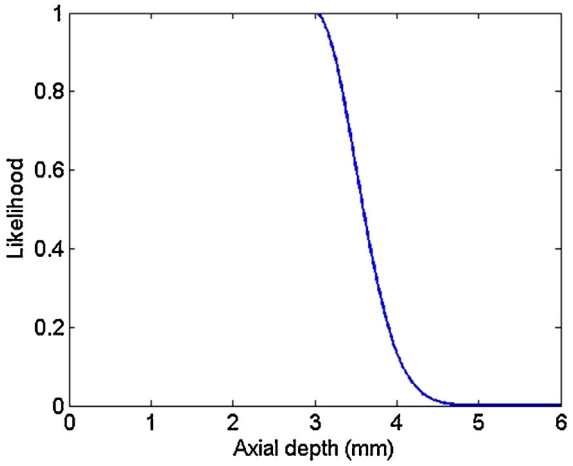

Fig. 10. Likelihood given an unstable result at 3 mm.

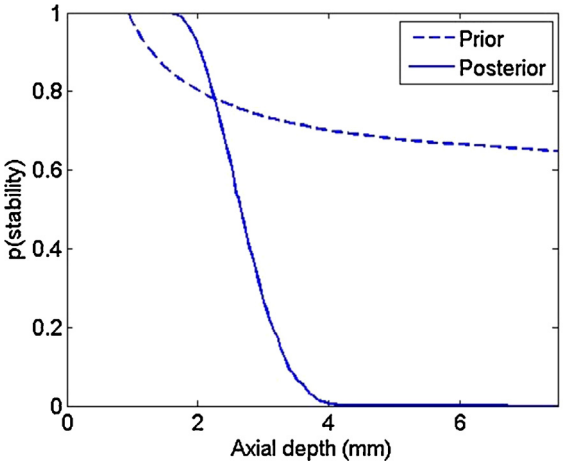

Fig. 12. Prior and posterior probability of stability at 400 rpm.

4.3. Bayesian updating

The posterior probability of each path is obtained by multiplying the prior and likelihood and normalizing such that the sum of all probabilities is equal to unity. The posterior probabilities of sample paths are used to calculate the posterior distribution of the process damping and cutting force coefficients. The experimental results shown in Fig. 4 were used to update the prior cdf of stability. For each experiment, the likelihood function was calculated using Eqs. (4) and (5) for a stable and unstable result, respectively. For multiple updates, the prior after the first update becomes the posterior after the second update and so on. Fig. 11 shows the posterior cdf given the experimental results. Stable results are denoted as 'o' and unstable results as 'x'. Figs. 12 and 13 show the prior and posterior probability of stability at 400 rpm and 1000 rpm, respectively.

After each update, the posterior mean and standard deviation of C was calculated using Eqs. (6) and (7).

$$\mu_c = \sum CP(C) \tag{6}$$

$$\sigma_c = \sum (C - \mu_c)^2 P(C) \tag{7}$$

In these equations, μ_C and σ_C are the mean and standard deviation of C, respectively, and $P(C)$ is the probability of the sample stability limit. Recall that each sample stability limit is generated from a sample of $\{K_t, K_n, C\}$. The probability of a sample stability limit is equal to the probability that the sample corresponds to the true limit.

For the prior, each sample stability limit was assumed to be equally likely to be the true limit; this implies that each $\{K_t, K_n, C\}$ sample was equally likely to be the true combination. The updated probability of each sample stability limit gives the updated probability of the underlying $\{K_t, K_n, C\}$ sample to be the true combination. The updated posterior probabilities of sample paths were used to calculate the posterior mean and standard deviation of C using Eqs. (6) and (7), respectively. Figs. 14 and 15 show the progression of μ_C and σ_C as a function of the number of tests. The μ_C and σ_C values after 50 tests were 2.49×10^5 N/m and 0.30×10^5 N/m, respectively. The value of C from the *RSS* method was 2.5×10^5 N/m. Figs. 14 and 15 show a convergence in μ_C and σ_C to the final values after the 18th test. The μ_C and σ_C values after the 18th test were 2.41×10^5 N/m and 0.34×10^5 N/m, respectively. This is due to the first unstable result at {400 rpm, 3 mm axial depth} preceded by a stable result at {400 rpm, 2.5 mm axial depth}. A stable result at a 2.5 mm axial depth and an unstable result at a 3 mm axial depth imply that there is a high probability that the true stability limit is between the two values. Also, note that the values remain approximately constant after subsequent updates.

The updating procedure was repeated for the 19.05 mm diameter, 11° relief angle tool. The prior marginal distribution

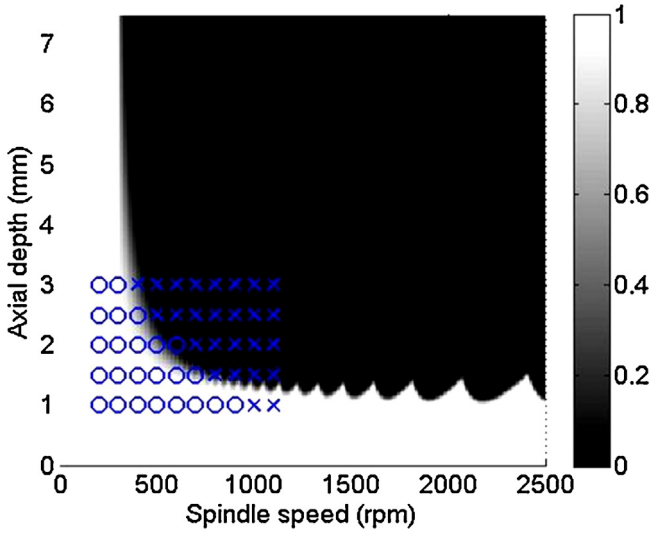

Fig. 11. Posterior cdf of stability. Stable results are denoted as 'o' and unstable results as 'x'.

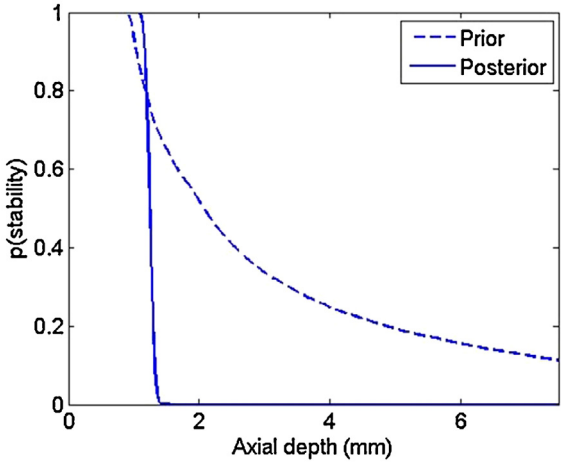

Fig. 13. Prior and posterior probability of stability at 1000 rpm.

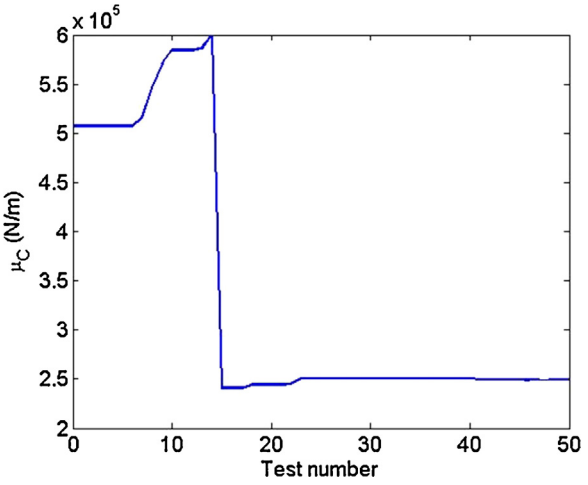

Fig. 14. μ_C as a function of the number of tests.

of the force coefficients were $K_t = N(2234.9,\ 107.0)\,\text{N/mm}^2$ and $K_n = N(1188.2,\ 40.5)\,\text{N/mm}^2$.The prior marginal distribution of C was again selected to be uniform, $U(0.5 \times 10^5,\ 10 \times 10^5)\,\text{N/m}$, and the coefficients were assumed to be independent of each other. The updating procedure was performed using the experimental results shown in Fig. 5. Fig. 16 shows the posterior cdf given experimental results. Figs. 17 and 18 show the progression of μ_C and σ_C as a function of the number of tests. The μ_C and σ_C values after 55 tests were 3.63×10^5 N/m and 0.38×10^5 N/m, respectively. The C value from the *RSS* method was 3.3×10^5 N/m. These results show good agreement between the posterior mean C and the value obtained using the *RSS* method. The advantage of using Bayesian inference over *RSS* is that the uncertainty in C can also be calculated. As a result, the stability boundary is not deterministic, but characterized by a cumulative probability distribution. In addition, Bayesian inference enables the value to be gained from performing an experiment to be calculated; this is described in the next section.

5. Experimental design using a value of information approach

Bayesian updating of the probability of stability and the process damping coefficient was demonstrated. Using experimental results, the probability of each sample stability limit being the true limit was updated. These probabilities were, in turn, used to

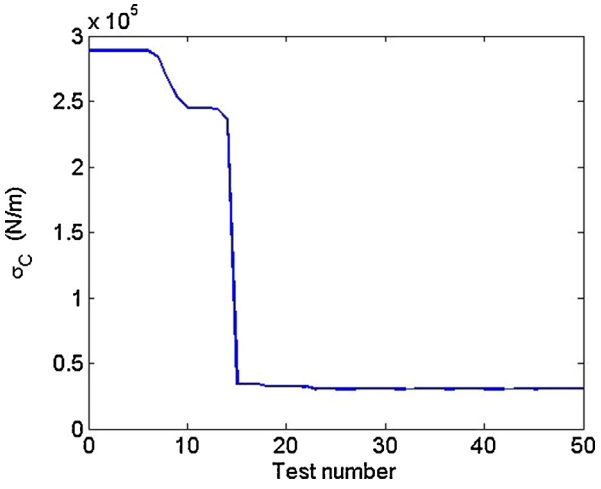

Fig. 15. σ_C as a function of the number of tests.

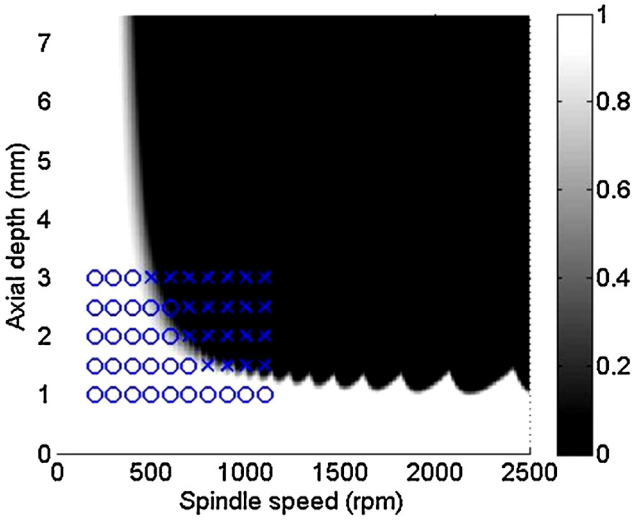

Fig. 16. Posterior cdf of stability. Stable results are denoted as 'o' and unstable results as 'x'.

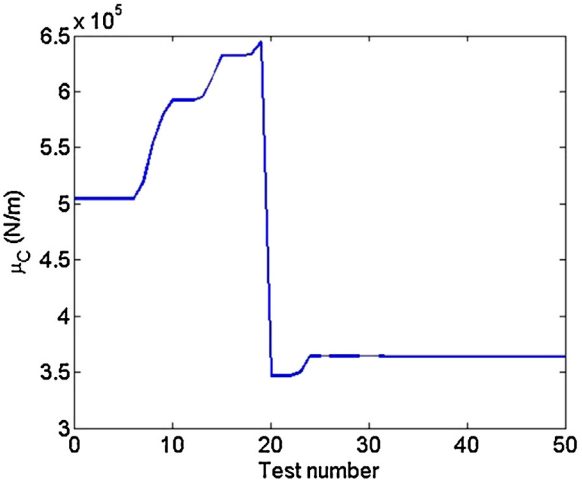

Fig. 17. μ_C as a function of the number of tests.

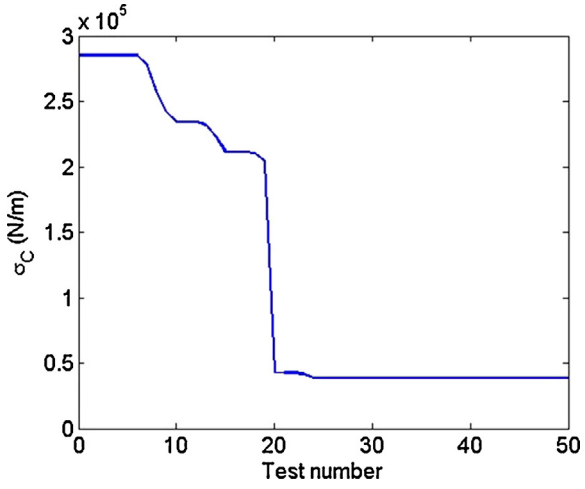

Fig. 18. σ_C as a function of the number of tests.

determine the posterior distribution of the process damping coefficient. The posterior mean agreed with the deterministic value calculated using the *RSS* method. Note that additional experimental results reduce the uncertainty (or the standard deviation) in the C value.

This section describes a value of information approach for optimal experimental parameter selection. The objective of the experiments is to reduce the uncertainty in the C value. Note that no new information (or reduction in uncertainty) is achieved by obtaining a stable result at a {spindle speed, axial depth} combination which has a prior probability of stability equal to one. A probability of stability equal to one indicates that all sample paths have a value of axial depth greater than the test axial depth at the test spindle speed. A stable result assigns a likelihood of one to all the sample stability limits, which results in no reduction in the value of σ_C. This is observed in Figs. 15 and 18 for the first five tests. On the other hand, a test at a combination which has a non-zero probability of stability will cause a reduction in σ_C due to the small likelihood value assigned to some sample paths.

The information from a test is characterized as an expected percent reduction in the value of σ_C. The experimental parameters are selected where the expected percent reduction in σ_C is maximum. To illustrate, consider four possible experimental {spindle speed, axial depth} combinations: A = {400 rpm, 1.28 mm}, B = {1000 rpm, 2.68 mm}, C = {1500 rpm, 2.04 mm} and D = {2000 rpm, 1.36 mm}. The probability of stability for test points A, B, C and D are 0.9, 0.5, 0.1, and 0.52, respectively (see Fig. 19).

Consider test point A. Given a stable or unstable result at point A, the posterior probabilities of the sample stability limits is updated using the procedure described previously. The posterior probabilities are used to calculate the values of μ_C of and σ_C via Eqs. (6) and (7). If the result at point A is stable, the value of σ_C would be 2.72×10^5 N/m. Note that the value of σ_C before any testing was 2.87×10^5 N/m. Therefore, the percent reduction in σ_C would be 5.60. On the other hand, if the result at point A was unstable, the value of σ_C would be 3.47×10^4 N/m giving a percent reduction of 87.9. Recall that point A has a 0.9 probability of being stable. The expected percent reduction in σ_C for point A is calculated as:

$$(\%\,\text{reduction in}\,\sigma_C)_A = 0.9 \times 5.60 + 0.1 \times 87.9 = 13.8.$$

The procedure was repeated for points B, C and D. The results are summarized in Table 2. As noted, points A and C have a high prior probability of being stable and unstable, respectively. As a result, the expected percent reduction in σ_C for testing at these points is low. On the other hand, points B and D have maximum uncertainty regarding the result, $p(\text{stability}) \sim 0.5$. Also, the distribution (or the uncertainty) in axial depth at point B (1000 rpm) is higher as compared to point D (200 rpm) as seen from Fig. 19. Therefore, the expected percent reduction is greater for testing at point B than point D.

Table 2
Expected percent reduction at test points.

Test	p(stability)	Expected percent reduction in σ_C
A	0.9	13.8
B	0.51	45.6
C	0.1	14.6
D	0.52	24.9

The {spindle speed, axial depth} domain was divided into a grid with increments of 50 rpm and 0.15 mm. The expected percent reduction in σ_C was calculated at all grid points using the procedure described. The maximum expected percent reduction was 49.6 at {550 rpm, 7.5 mm} with a probability of stability equal to 0.51. The test result was selected to be unstable based on the stability limit displayed in Fig. 4. The purpose of using the stability limit in Fig. 4 to determine the test result was to validate the convergence of the posterior mean and standard deviation of C to the values determined using the original 50 tests. The values of μ_C and σ_C after the first update were 2.53×10^5 N/m and 1.42×10^5 N/m, respectively. The posterior after the first update becomes the prior for the second update. The procedure to calculate value of information was repeated for the second test. The maximum expected percent reduction was 48.3 at {550 rpm, 3.0 mm} with a probability of stability equal to 0.54. The values of μ_C and σ_C after the second update were 3.63×10^5 N/m and 0.79×10^5 N/m, respectively. With each update using experimental result, there is reduction in the σ_C values as seen from the first two experimental results. Therefore, the maximum expected reduction in σ_C will also reduce for every subsequent test. The maximum percentage reduction in the process damping coefficient uncertainty was used as a stopping criterion for doing experiments. It was decided that an experiment is only worthwhile if the expected reduction in σ_C is at least 10.

The procedure was repeated till the maximum expected reduction in σ_C was less than 10. The test results were all based on the stability limit shown in Fig. 4. As noted, the test points were selected where the expected percent reduction in C was maximum. Fig. 20 shows the maximum expected percent reduction in C for each test. As seen in the figure, the percent reduction in σ_C is 8.3 for the

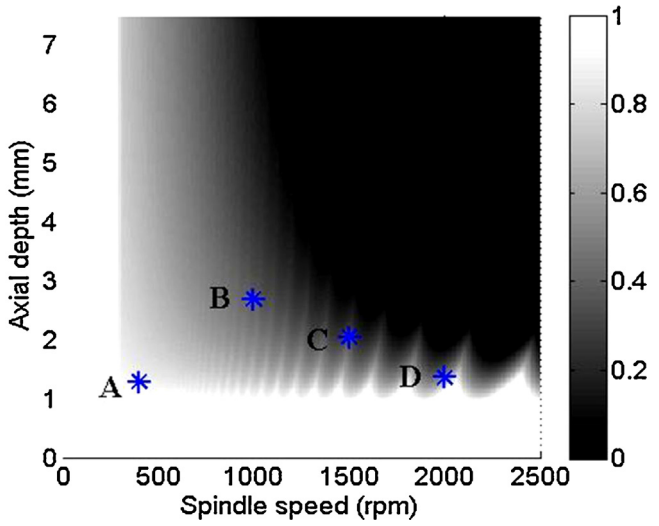

Fig. 19. Four possible test points.

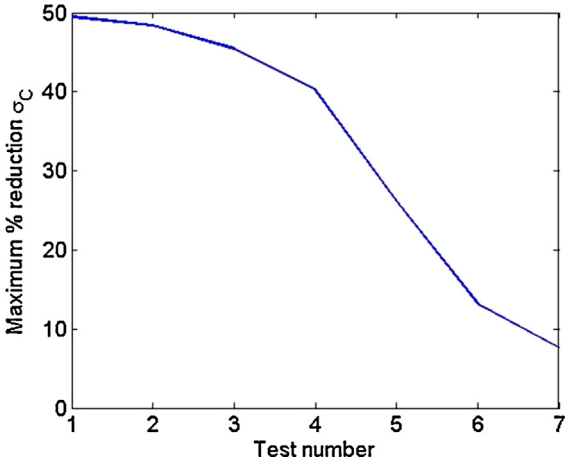

Fig. 20. Maximum expected percent reduction for each test.

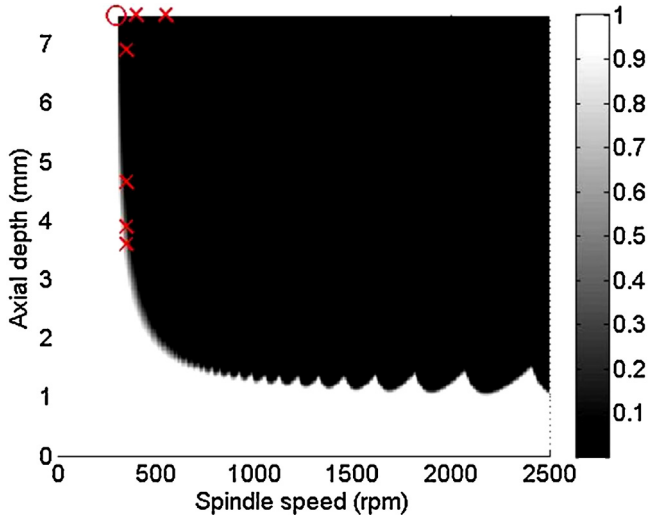

Fig. 21. Posterior cdf of stability. Stable results are denoted as 'o' and unstable results as 'x'.

Table 3
Experimental results.

Spindle speed (rpm)	Axial depth (mm)	Result
550	7.5	Unstable
300	7.5	Stable
400	7.5	Unstable
350	6.9	Unstable
350	4.65	Unstable
350	3.9	Unstable
350	3.6	Unstable

seventh test. The seventh experiment was performed and the procedure was terminated. Fig. 21 shows the posterior cdf after seven updates. Stable results are denoted as 'o' and unstable results as 'x'. Table 3 lists the experimental test points and the stability results for all seven tests. Figs. 22 and 23 show the progression of μ_C and σ_C as a function of the number of tests. Note that the mean converges to 2.5×10^5 N/m in seven tests as compared to 50 tests as shown in Fig. 14. An alternate criterion for stopping is to calculate the percentage reduction in σ_C from the prior (before any testing) value. If the location of the boundary was known with certainty, the value of σ_C would be zero. Therefore, the maximum percentage reduction in σ_C achievable by testing is 100. This value is also referred to as the value of perfect information. The value of perfect

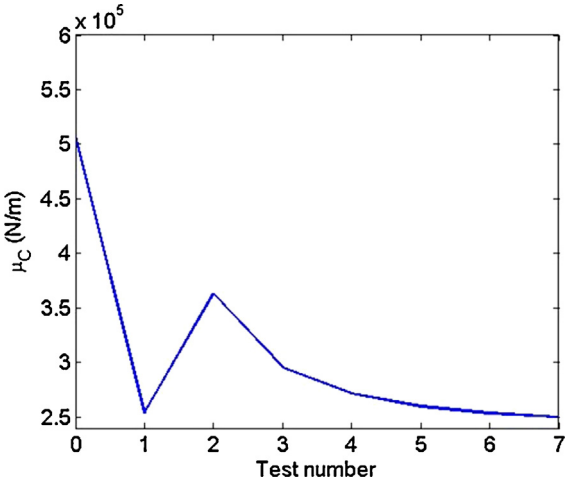

Fig. 22. μ_C as a function of the number of tests.

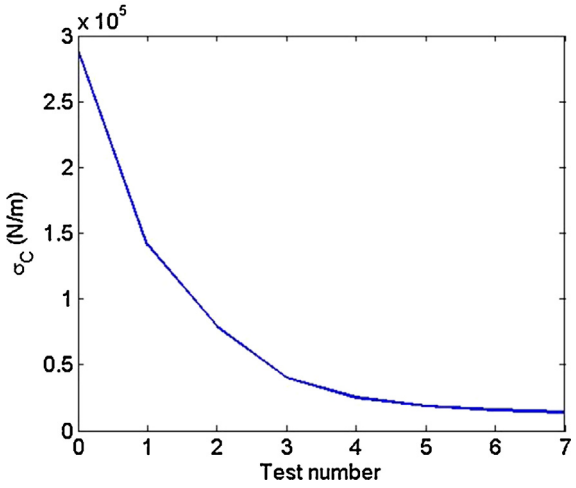

Fig. 23. σ_C as a function of the number of tests.

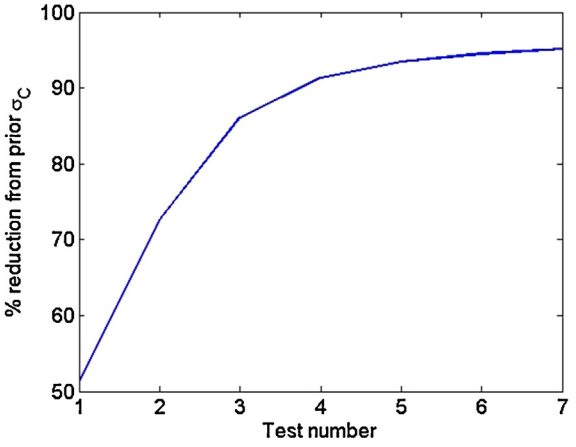

Fig. 24. Percent reduction in σ_C from the prior value.

information implies that any experimentation is not worthwhile if the cost of experiments exceeds the value of perfect information [3,4]. The value of perfect information can be calculated a priori to decide if any experiments should be performed. However, the user

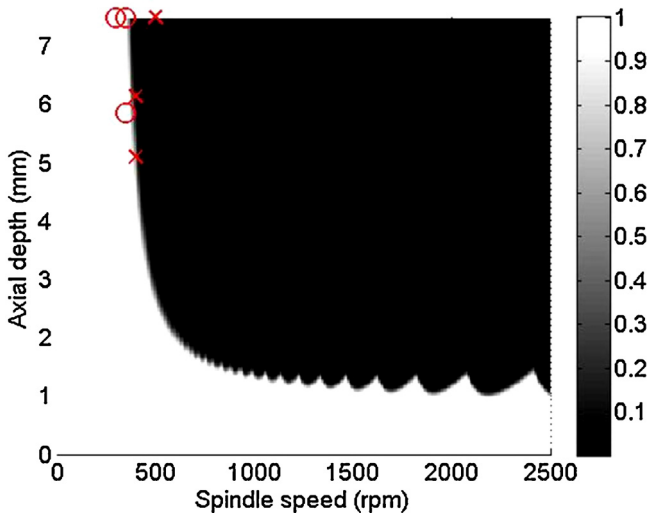

Fig. 25. Posterior cdf of stability. Stable results are denoted as 'o' and unstable results as 'x'.

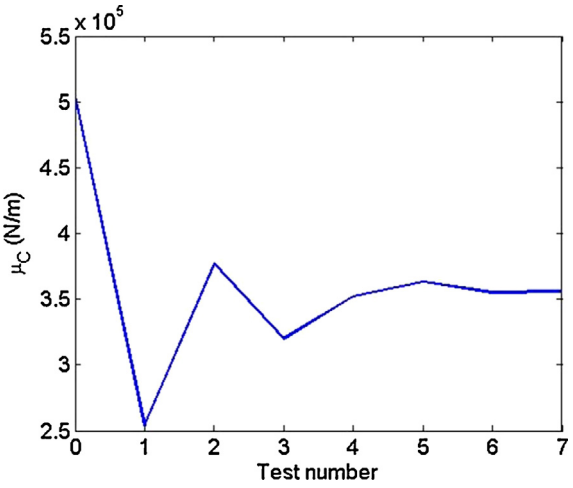

Fig. 26. μ_C as a function of the number of tests.

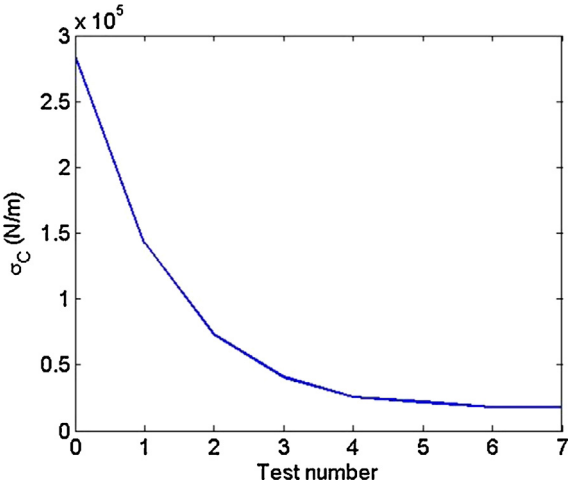

Fig. 27. σ_C as a function of the number of tests.

can decide that no additional experimentation is required after a certain percentage reduction in the prior σ_C value (such as 90) is achieved. Fig. 24 shows the percentage reduction in σ_C from the before testing value as a function of number of tests.

The experimental selection procedure was repeated for the 19.05 mm diameter, 11° relief angle tool. Seven tests were performed at points where the expected percent reduction in σ_C was maximum. Fig. 25 shows the posterior cdf. Stable results are denoted as 'o' and unstable results as 'x'. Figs. 26 and 27 display the progression of μ_C and σ_C as a function of the number of tests. Note that the mean converges to 3.6×10^5 N/m in seven tests.

6. Conclusions

A random walk method of Bayesian updating was demonstrated for process damping coefficient identification. The prior sample paths were generated using an analytical process damping algorithm. For the prior, each sample stability limit was assumed to be equally likely to be the true stability limit. The probability of the sample stability limit was then updated using experimental results. The updated probabilities of the sample paths were used to determine the posterior process damping coefficient distribution. A value of information was used to select experimental test points which maximized the expected reduction in the process damping coefficient uncertainty. Results show a significant decrease in the number of tests required as compared to DOE. To illustrate, for two parameters and five levels, the Taguchi method requires 25 experiments. Similarly, the central composite design requires 15 experiments. The value of information method converges to the true value in seven tests. In addition, the range and the number of levels selected may not result in the identification of the process damping coefficient. The value of information method is robust and uses a normative criterion for experimental design. The value of information considers the value on uncertainty reduction in selecting the experimental parameters, in addition to serving as a stopping criterion for additional testing.

References

[1] Hicks C, Turner Jr K. Fundamental concepts in the design of experiments. New York, NY: Oxford University Press; 1999.
[2] Jiju A. Design of experiments for engineers and scientists. Burlington, MA: Elsevier Ltd.; 2003.
[3] Howard R. Information value theory. IEEE Trans Syst Sci Cybern 1966;2(1):22–6.
[4] Howard R. Decision analysis: perspectives on inference, decision and experimentation. Proc IEEE 1970;58(5):632–43.
[5] Howard R. Decision analysis: applied decision theory. In: Proceedings of the 4th international conference on operational research. 1966. p. 55–7.
[6] Tlusty J, Polacek M. The stability of machine tools against self-excited vibrations in machining. In: Proceedings of the ASME international research in production engineering conference. 1963. p. 465–74.
[7] Tobias SA. Machine tool vibrations. Glasgow: Blackie and Sons, Ltd.; 1965.
[8] Tlusty J, Zaton W, Ismail F. Stability lobes in milling. Ann CIRP 1983;32/1:309–13.
[9] Altintas Y, Budak E. Analytical prediction of stability lobes in milling. Ann CIRP 1995;44/1:357–62.
[10] Wallace PW, Andrew C. Machining forces: some effects of tool vibration. J Mech Eng Sci 1965;7:152–62.
[11] Sisson TR, Kegg RL. An explanation of low-speed chatter effects. J Eng Ind 1969;91:951–8.
[12] Peters J, Vanherck P, Van Brussel H. The measurement of the dynamic cutting coefficient. Ann CIRP 1971;21/2:129–36.
[13] Tlusty J. Analysis of the state of research in cutting dynamics. Ann CIRP 1978;27/2:583–9.
[14] Wu DW. A new approach of formulating the transfer function for dynamic cutting processes. J Eng Ind 1989;111:37–47.
[15] Elbestawi MA, Ismail F, Du R, Ullagaddi BC. Modelling machining dynamics damping in the tool–workpiece interface. J Eng Ind 1994;116:435–9.
[16] Lee BY, Trang YS, Ma SC. Modeling of the process damping force in chatter vibration. Int J Mach Tools Manuf 1995;35:951–62.
[17] Huang CY, Wang JJ. Mechanistic modeling of process damping in peripheral milling. J Manuf Sci Eng 2007;129:12–20.
[18] Ahmadi K, Ismail F. Experimental investigation of process damping nonlinearity in machining chatter. Int J Mach Tools Manuf 2010;50:1006–14.
[19] Budak E, Tunc LT. A new method for identification and modeling of process damping in machining. J Manuf Sci Eng 2009;131. pp. 051019/1–10.
[20] Altintas Y, Eynian M, Onozuka H. Identification of dynamic cutting force coefficients and chatter stability with process damping. Ann CIRP 2008;57/1:371–4.
[21] Tyler C, Schmitz T. Process damping analytical stability analysis and validation. Proc NAMRC/SME 2012;40.
[22] Tlusty J. Manufacturing processes and equipment. Upper Saddle River, NJ: Prentice Hall; 2000.